Environmental Science and Pollution Research (2023) 30:36872–36882
https://doi.org/10.1007/s11356-022-24900-x

RESEARCH ARTICLE

Magnetic seeds promoted high-density sulfonic acid-based hydrochar derived from sugar-rich wastewater for removal of methylene blue

Xuelei Jiang[1,2] · Yuyao Jia[1] · Dezhang Ren[1] · Nahui Zhang[1] · Tao Peng[3] · Zhibao Huo[1]

Received: 11 September 2022 / Accepted: 16 December 2022 / Published online: 23 December 2022

Abstract

Methylene blue (MB) removal from dyeing wastewater using low-cost bio-derived adsorbent is a significant and challenging field. Herein, magnetic sugar hydrochar (MGHC) precursors derived from sugar-rich wastewater with small particle size and rich oxygen-containing functional groups (OCFGs) are prepared from sugar-rich aqueous solution via Fe salt-modified hydrothermal procedure. The role of Fe_3O_4 nanoparticles formed during the sugar carbonization is to provide numerous magnetic seeds to generate MGHC with core–shell structure, which reduces the particle size of hydrochar. This increases the amount of OCFGs on the surface of MGHC for bonding the sulfonic acid groups. Therefore, sulfonic acid-modified MGHC-SA shows the rapid MB adsorption rate and excellent adsorption capacity. The highest MB capacity is 869.6 mg/g at pH = 11.0 and 298 K. Additionally, the MGHC-SA can be easily recovery by magnet. And the stability of MGHC-SA was also evaluated, no degradation of adsorption performance was observed, even the adsorbent was regenerated 10 times. This study puts forward a promising way to acquire functional groups rich and easy recovery hydrochar from sugar wastewater for MB removal.

Keywords Sugar-rich wastewater · Hydrothermal reaction · Biochar · Magnetic adsorbent · Sulfonic acid group · Methylene blue

Introduction

Organic dye effluent is one of the major sources of water pollution, which is highly toxic and difficult to be degraded by biochemical treatment (Anuma et al. 2021; Methneni et al. 2021; Samuchiwal et al. 2021; Varjani et al. 2021). As a representative of dye pollutants, methylene blue (MB) removal in industrial wastewater has been widely studied for several decades (Jawad et al. 2019; Li et al. 2018, 2021; Zhang et al. 2021). Although advanced oxidation techniques (AOT) have been proved to be extraordinarily effective at breaking MB molecules (Dong et al. 2021; Javanbakht & Mohammadian 2021), great concerns of economic and environmental issues (energy intensive, reagent addition, sludge, etc.) caused by AOT have been paid for many years (Ismail & Sakai 2022; Wolski et al. 2021; Wu et al. 2022). Therefore, removing MB from wastewater via adsorption process is another feasible and mainstream strategy possessing low operation cost and good removal effect of organic matters (Bhadra & Jhung 2020; Cheng et al. 2021; Zhang et al. 2020). In general, the key of adsorption treatment is to develop high adsorption capacity, easy recovery, reproducible, and low-cost adsorbent (Deng et al. 2019; Gao et al. 2019; Phetphaisit et al. 2016; Qu et al. 2021; Zhao et al. 2020).

Biochar is a kind of promising candidate adsorbents, which is prepared via thermal treatment of biomass materials such as pyrolysis and hydrothermal carbonization process (Gusain et al. 2020; Viotti et al. 2019). Currently, sugar-rich wastewater is typical biomass waste in the southwest of China where sugar industry is rather prevalent (Zeydouni et al. 2018). Traditional biotreatments are widely used to degrade organic

Responsible Editor: Zhihong Xu

Xuelei Jiang, Yuyao Jia, and Dezhang Ren contributed equally.

✉ Zhibao Huo
zbhuo@shou.edu.cn

[1] College of Marine Ecology and Environment, Shanghai Ocean University, 999 Huchenghuan Road, Shanghai 201306, China

[2] Shanghai Urban Construction Water Engineering Co., Ltd, 291 Wenshui East Road, Shanghai 200434, China

[3] Institute of Geochemistry, Chinese Academy of Science, 99 Lincheng Road West, Guiyang 550081, China

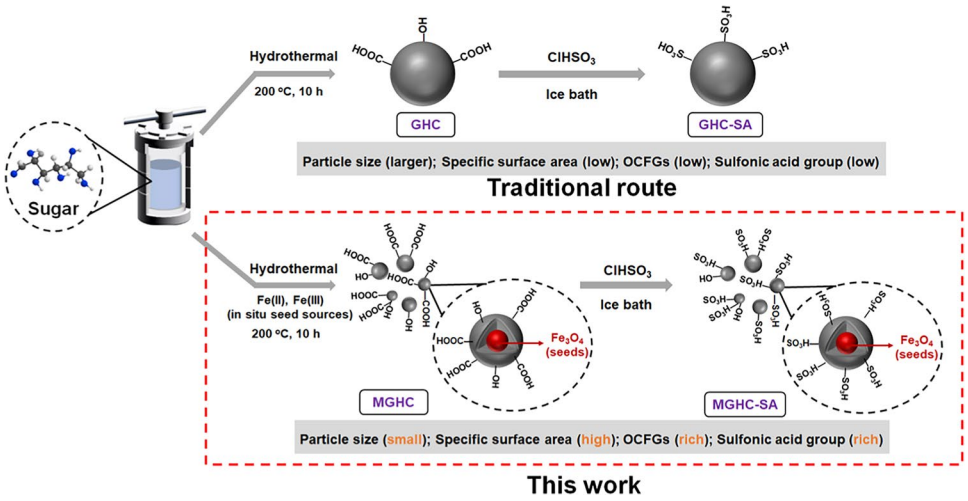

Scheme 1 Schematic diagram of material synthesis

matters in sugar-rich wastewater (Li et al. 2020; Pirsaheb et al. 2020), which results in waste of valuable carbon resources (Karray et al. 2017; Kumar et al. 2021; Li et al. 2016; Liu et al. 2021; Oliveira et al. 2021). Consequently, hydrothermal conversion of biomass waste including concentrated sugar water into value-added hydrochar (HC) is a promising and eco-friendly approach which has been verified in recent years (Han et al. 2018, Yang and Cannon 2021).

In most cases, the adsorption performance of raw biochar is greatly inferior to other commercial adsorbents. As a result, modification of biochar is necessary to create more and higher active sites for enhancing the adsorption process of pollutant molecules (Li et al. 2019b; Lu et al. 2021, Wang and Wang 2019). Therefore, numerous studies, at present, have focused on raising specific surface area and introducing efficient functional groups on the surface of materials to achieve ideal carbon-based adsorbents. Introduction of functional groups into carbon adsorbents is a useful method to adjust surface characteristics of materials, which is crucial for adsorption performance (Caldera Villalobos et al. 2016; Han et al. 2018; Li et al. 2019a; Zhang et al. 2013). In order to attach stable functional groups on biochar surface, oxidation of biochar with oxidizing agents such as H_2O_2, $KMnO_4$, and HNO_3 is a common and easy technique to generate oxygen-containing functional groups (OCFGs) which can be used as anchors to attach highly active groups (Mehmood et al. 2021; Yang et al. 2021; Zhang et al. 2021; Zheng et al. 2021). However, employing corrosive oxidizing agents increases the operational cost and environmental risks. Unlike biochar prepared by other thermal treatments, HC obtained via hydrothermal carbonization owns abundant intrinsic hydroxy and carboxyl groups (Wang et al. 2019). Nevertheless, in view of the feature of HC derived from sugar-rich wastewater, the specific surface area of this HC is relatively low, which inhibits the amount of active functional groups (Higgins et al. 2020; Marzbali et al. 2021).

Typically, biochar treated with etching additives such as KOH and $ZnCl_2$ at high temperature is able to access high specific surface area and extensively porous structure (Islam et al. 2017; Luo et al. 2019b). However, corrosive and heavy metal vapors release during the thermal treatment increasing the cost of exhaust gas equipment. Otherwise, physical route such as ball milling of biochar is also an efficient process which has been reported in recent years. In spite of this, thermal treatment and ball milling are likely to reduce the OCFGs in biochar. Based on above, in situ formation of porous HC by modifying with a green agent to induce sugar molecule carbonization specifically may be a viable solution (Luo et al. 2019a; Masunga et al. 2019).

Herein, complex Fe salts were introduced into sugar aqueous solution which was used as simulated sugar-rich wastewater, and in situ generated Fe_3O_4 nanoparticles offer seeds for sugar carbonization during hydrothermal process to form HC with core–shell structure (Scheme 1). Notice that adsorbent with Fe_3O_4 core makes the recovery convenient and fast by magnet. The as-prepared HC (MGHC) has much larger specific surface area and higher density of OCFGs than that of raw one (GHC). Therefore, MGHC-SA modifying with sulfonic acid group exhibits excellent MB adsorption capacity (869.6 mg/g) which is approximately 13 times higher than of the GHC-SA. Moreover, MGHC-SA presents good recyclability and no deactivation was observed after 10 times reuse.

Materials and methods

Materials

Materials used were D-glucose anhydrous (GR), ferric chloride anhydrous (AR), ferrous chloride anhydrous (AR), urea (AR), chlorosulfonic acid (AR), dichloromethane

(AR), hydrochloric acid (0.1 mol/L), sodium hydroxide (0.1 mol/L), and methylene blue ($C_{16}H_{18}ClN_3S{\cdot}3H_2O$). Deionized water was used throughout the experiment.

Synthesis of adsorbent

Synthesis of magnetic sugar hydrothermal carbon (MGHC) was follows: first, 6 g of glucose, 3 g of urea, 1.2 g of $FeCl_3$, 0.6 g of $FeCl_2$, and 60 mL of H_2O were added together to 100 mL of liner, stirred thoroughly, and then placed in a stainless steel autoclave and heated to 200 °C, and reacted for 10 h. The obtained MGHC was washed twice with ethanol and deionized water and then dried in an oven at 60 °C for 12 h. Other hydrothermal carbon materials including GHC and GHC-H_2O_2 were also prepared as shown in Supporting Information (S1).

Synthesis of sulfonic acid-based magnetic sugar hydrothermal carbon (MGHC-SA) (Goswami and Phukan 2017, Naeimi and Mohamadabadi 2014) was as follows: first, 1 g MGHC was added to 20 mL dichloromethane and sonicated for 30 min. 1 mL $ClHSO_3$ was added to the ice-cold dispersion of MGHC and reacted at room temperature for 30 min. After the addition was completed, the mixture was stirred thoroughly for 3 h to allow complete evaporation of HCl from the vessel. Then, MGHC-SA was separated from the mixture using a magnetic field and washed twice with ethanol and deionized water. Finally, it was dried in an oven at 60 °C for 12 h. Sulfonated sugar hydrothermal carbon (GHC-SA) and sulfonated hydrogen peroxide-treated sugar hydrothermal carbon (GHC-H_2O_2-SA) were prepared using the same method.

The method of characterization of the material can be seen in the Supporting Information (S2).

Methylene blue adsorption experiments

MB stock solution (1000 mg/L) was prepared by dissolving 1 g of MB in 1 L of H_2O. The fresh stock solution was then diluted to a specific concentration (100–600 mg/L) for the experiment. 100 mg of adsorbent was added to 100 mL of a specific concentration of methylene blue solution, and the solution was shaken in a thermostatic shaker for several hours at a certain temperature; then, the solution was filtered using a 0.45-μm membrane and the concentration of MB in the filtrate was detected using a UV–Vis spectrophotometer with λ_{max} at 664 nm. Other experiments including effect of pH, the adsorption isotherm experiments, kinetic analysis, and adsorption–desorption experiments could be seen in Supporting Information (S3).

Results and discussions

Characterization of the synthesized materials

In order to verify the core–shell structure of MGHC, morphologies of GHC, MGHC, and nano Fe_3O_4 were analyzed by scanning electron microscope (SEM) and transmission electron microscope (TEM). As shown in Fig. 1a and Fig. S1a, GHC is assembled with micron-sized carbon spheres, whereas numerous nanoparticles combined with bits of micron-sized spheres are observed in MGHC (Fig. S1b). High multiple SEM image in Fig. 1b shows that these nanoparticles attach on the surface of carbon spheres. By comparing the X-ray diffraction (XRD) patterns of GHC and MGHC in Fig. S2, diffraction peaks at 34.5°, 36.5°, and 42.0° are discovered in MGHC proving the existence of Fe_3O_4 (Luo et al. 2019a). Moreover, because the size of nano Fe_3O_4 prepared via the same hydrothermal process are close to the nanoparticles in MGHC (Fig. 1c), it can be inferred that the structure of nano Fe_3O_4 core covering with carbon shell is formed during the glucose carbonization. This is further confirmed by the TEM and high-resolution TEM (HRTEM) images of MGHC in Fig. 1d 10–20 nm particles buried in amorphous carbon shell are clearly observed and the lattice fringes on single nanoparticle with *d*-spacing of 0.296 nm correspond to Fe_3O_4 (220) plane (Fang et al. 2020).

N_2 adsorption–desorption tests were conducted to get insight into the influence of the modification of Fe salts for the specific surface area and pore size distribution of GHC and MGHC. As shown in Fig. 2a, higher adsorption volume of MGHC than that of GHC is observed, which demonstrates the MGHC has higher specific surface area. The detailed data of GHC and MGHC are 0.58 m^2/g and 4.73 m^2/g, respectively. Furthermore, the *d* majority of pores in MGHC with diameter ranges from 2 to 10 nm, whereas the distribution of pore size in GHC is over 10 nm (Fig. 2b). As stated above, Fe_3O_4 nanoparticles formed during the hydrothermal process offer seeds to generate MGHC with core–shell structure reducing the size of GHC particles, which is conductive to afford more OCFGs as grafting sites on the surface of HC.

Subsequently, functional groups in GHC and MGHC were analyzed by Fourier transform infrared spectroscopy (FT-IR). As shown in Fig. 3a, peaks at 3257 cm^{-1} and 1699 cm^{-1} are assigned to the stretching vibrations of OH and C = O groups (Deng et al. 2019; Li et al. 2019c), respectively, which suggests the presence of OCFGs in both GHC and MGHC. In addition, a new peak at 640 cm^{-1} in MGHC corresponding to vibration of Fe–O bond attributes to the Fe_3O_4 nanocore. Other than that, X-ray photoelectron spectroscopy (XPS) was conducted

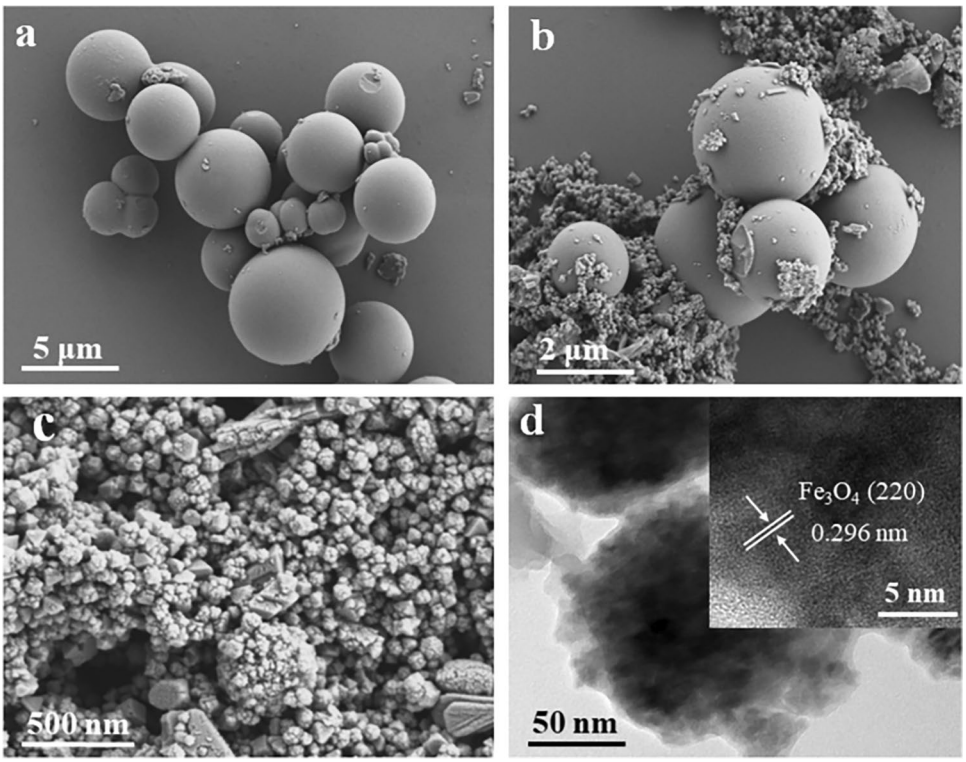

Fig. 1 SEM images of (**a**) GHC, (**b**) MGHC, (**c**) Fe3O4, and (**d**) TEM image of MGHC

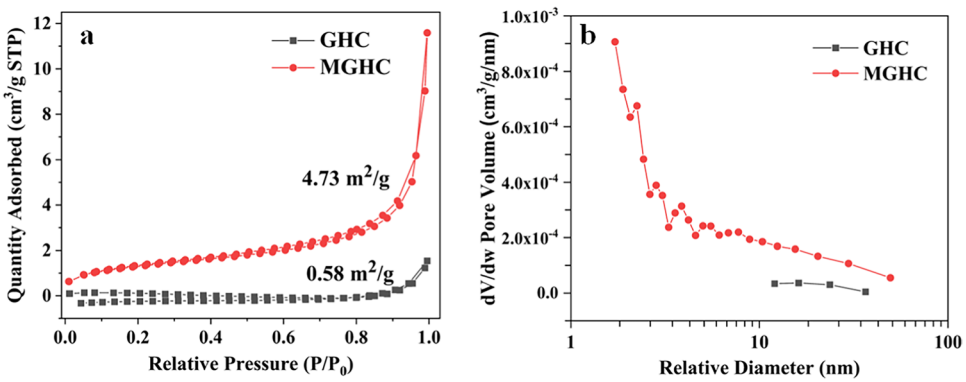

Fig. 2 **a** N2 adsorption–desorption isotherm. (**b**) Pore size distribution of GHC and MGHC

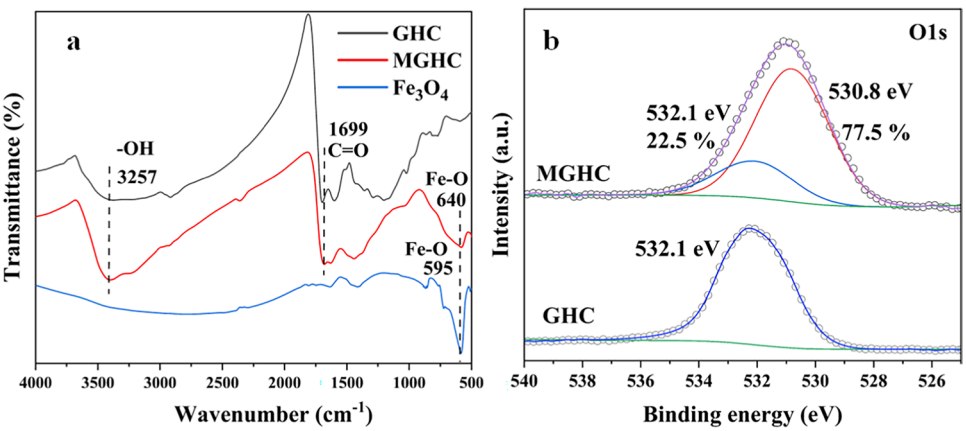

Fig. 3 **a** FT-IR spectra of GHC, MGHC, and Fe3O4. (**b**) O 1 s spectra of GHC and MGHC

to probe surface chemical state of as-prepared samples. The same as the FT-IR results, C and O signals are spotted in both survey profiles of GHC and MGHC, while Fe are only detected in MGHC (Fig. S3). High-resolution XPS spectra of O1s shows that the peaks located at 530.8 eV and 532.1 eV assign to lattice and adsorbed oxygen species (Liang et al. 2021; Wang et al. 2019; Zhang et al. 2021), respectively, which corresponds to Fe_3O_4 and OCFGs (Fig. 3b). Combined with morphology results, high mole ratio of adsorbed oxygen in MGHC (22.5%) demonstrates that the surface of MGHC is well covered with oxygen-rich carbon shell. For proper investigation of the amount of OCFGs on the surface of as-prepared HCs, Boehm titration method was applied to determine acidic groups which can reflect the content of OCFGs. As shown in Table 1, the amount of acidic groups in MGHC (22.4 mmol/g) is obviously higher than that of GHC (16.6 mmol/g). Indeed, ruling out the impact of the mass of Fe_3O_4 nanocore, Fe oxide-free MGHC, in theory, has higher acidic groups density (38.8 mmol/g).

Table 1 Content of oxygen-containing groups

Adsorbents	Oxygen-containing functional groups (mmol/g)			
	-COOH	-COOR	-OH	Total acidity
GHC	8.5	5.3	2.8	16.6
MGHC	0.06	20.0	2.3	22.4

For results outlined above, sulfonic acid groups as typical active adsorption sites were introduced to attach on GHC and MGHC via graft reaction between OCFGs and chlorosulfonic acid molecules. SEM images of MGHC-SA shown in Fig. 4a and Fig. S4 reveals that the morphology of MGHC-SA is maintained after modifying with chlorosulfonic acid. EDS elemental mapping shows that Fe, C, and S are dispersed homogeneously (Fig. 4b), indicating Fe_3O_4 nanoparticles are well buried into HC shell with rich sulfonic acid groups (Li et al. 2019b). Core–shell structure of MGHC-SA is also clearly observed via TEM and HRTEM images in Fig. 4c and d which demonstrates that Fe_3O_4 were preserved during the chlorosulfonic acid treatment (He et al. 2020; Qu et al. 2021). FT-IR spectra in Fig. S5 shows that MGHC-SA displays strong absorption peaks at 1182 and 1029 cm^{-1} which attribute to the asymmetric stretching of S = O and stretching vibrations of S–O, respectively (Dash et al. 2018). However, the peaks of S = O and S–O in GHC-SA are weak. This indicates that MGHC-SA contains higher density of sulfonic acid groups than the raw GHC. As a contrast, GHC was oxidized by H_2O_2 (named as GHC-H_2O_2) to increase the amount of OCFGs, then the chlorosulfonic acid modified GHC-H_2O_2-SA appears the obvious absorption peaks of S = O and S–O from FT-IR spectra, confirming the vital grafting role of surface OCFGs, which also demonstrates that Fe salts modification method is an effective strategy to construct HC with high-density active grafting sites. Other

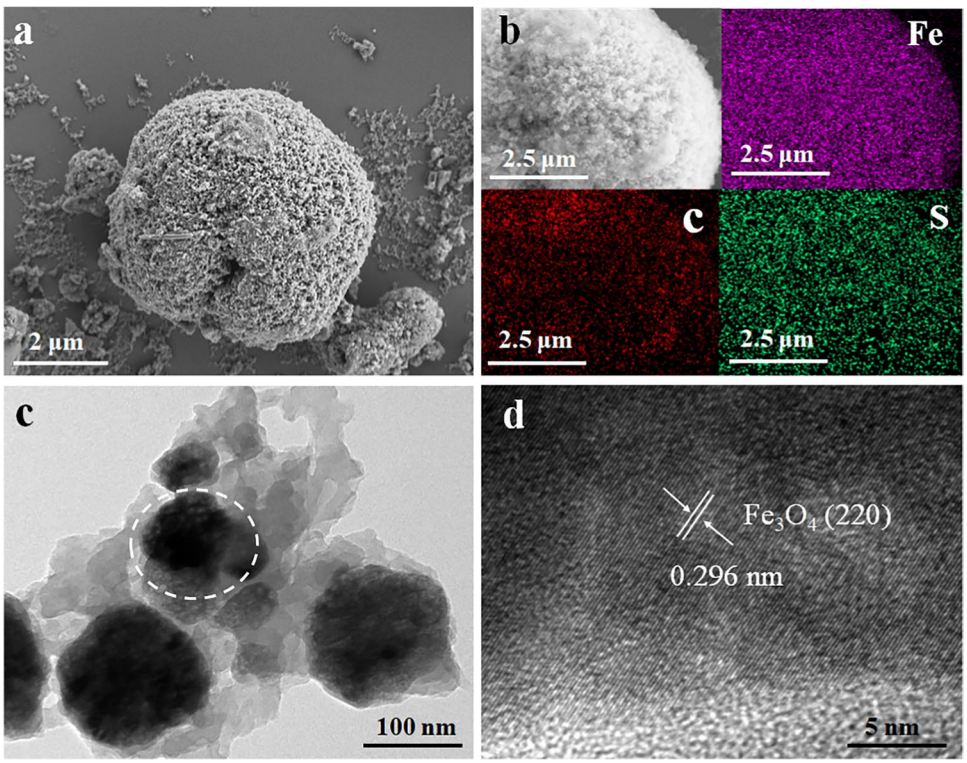

Fig. 4 SEM image of (**a**) MGHC-SA. (**b**) The corresponding elemental mapping of Fe, C, and S. (**c**) TEM and (**d**) HRTEM images of MGHC-SA

evidence comes from XPS results shown in Fig. S6. The mole ratio of S on the GHC-SA surface is 0.6%, which is lower than that of GHC-H_2O_2-SA (2.1%) and MGHC-SA (3.6%).

Saturation flux investigation was also conducted to analyze the magnetization intensity of as-prepared samples (Naeimi and Mohamadabadi 2014, Qu et al. 2021). The hysteresis regression curves in Fig. S7 shows that GHC, MGHC, and MGHC-SA with 0, 12.3, and 8.7 emu/g saturation magnetization intensity, respectively, illuminating in situ formed Fe_3O_4 nanoparticles afford magnetic source for HC. Although modest loss of magnetization intensity in MGHC-SA is observed which may be attributed to a spot of metal oxide leaching during the chlorosulfonic acid treatment, MGHC-SA still shows a good magnetic response in the case of external magnets (Fig. S7, inset), demonstrating the good potential which can be used as a recyclable magnetic sorbent (He et al. 2020).

Adsorption performance of as-prepared adsorbents

The adsorption performances of several as-prepared adsorbents for MB removal were investigated at pH = 7.0 and 298 K. As shown in Fig. 5, Fe_3O_4 nanoparticles barely adsorb MB, implying Fe_3O_4 cannot afford efficient adsorption sites for MGHC and MGHC-SA. The MB adsorption capacities of GHC, GHC-H_2O_2, and MGHC are 10.0, 10.5, and 18.0 mg/g, respectively. Raw GHC shows the inferior performance ascribing the low specific surface area and low density of OCFGs. Although oxidation treatment is favorable for increasing the amount of OCFGs, the adsorption capacity of GHC-H_2O_2 remains poor. According to SEM and N_2 adsorption–desorption

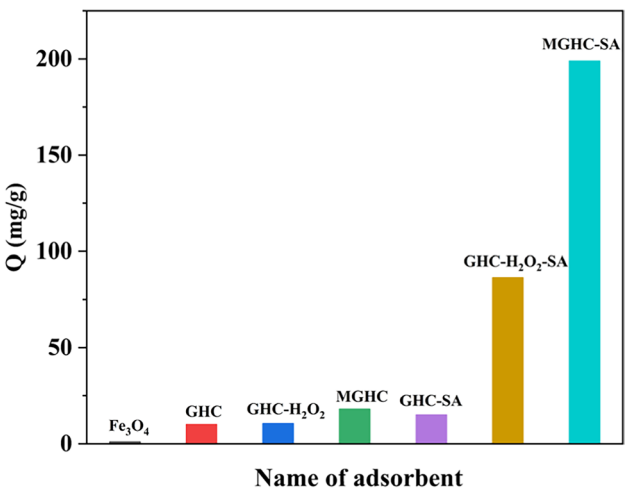

Fig. 5 Adsorption capacity of different materials for MB (C0 = 200 mg/L, V = 50 mL, m = 30 mg, pH = 7.0, and T = 298 K)

results (Fig. S8, S9), the particle size of GHC-H_2O_2 is still large, which leads to the low specific surface area. As expected, MGHC with abundant OCFGs exhibits the good MB adsorption performance. However, the performance of OCFGs is confined due to their internal property. The role of OCFGs in HC adsorbents were designed as grafting sites to fix sulfonic acid groups on the surface of adsorbents. Therefore, chlorosulfonic acid-treated GHC-SA, GHC-H_2O_2-SA, and MGHC-SA show better MB adsorption capacity than that of original HC adsorbents. Specifically, MB adsorption capacity of GHC-SA is 15.0 mg/g which is slightly higher than GHC, whereas GHC-H_2O_2-SA presents preferable MB removal effect (86.4 mg/g), even both GHC-SA and GHC-H_2O_2-SA contain the approximate specific surface area, manifesting the vital role of OCFGs for the performances of chlorosulfonic acid-modifying HC adsorbents. Hence, MGHC-SA shows the predictable highest MB adsorption capacity (199.0 mg/g) due to the precursor (MGHC) provides more OCFGs to immobilize active sulfonic acid groups.

Effect of pH

Because MB is a basic cationic dye, adsorbent with negative surface charge is in favor of the electrostatic adsorption of MB. Altering pH of aqueous solution can adjust the surface charge of MGHC-SA thanks to the existence of the abundant functional groups, especially sulfonic acid groups. In this regard, zeta potential was conducted to examine the surface charge of MGHC-SA at different pH values and probe the point of zero charge (pH_{PZC}) which is a specific pH where adsorbent contains charge neutrality surface (Li et al. 2021; Wang et al. 2018). As shown in Fig. 6a, zeta potential changes from positive to negative when pH increases from 2 to 12, and the pH_{PZC} of MGHC-SA is 6.8. Therefore, MGHC-SA in alkaline solution, specifically pH > 6.8, has plenty of negative surface charge due to deprotonation of sulfonic acid groups. It can be inferred that MGHC-SA possesses the good MB adsorption potential. Conversely, the grafting sulfonic acid groups on MGHC-SA will be protonated in acidic solution, which makes MGHC-SA positively charged and weakens the absorbability for MB.

On the basis of above analysis, the adsorption performances of MGHC-SA at different pH were explored. Figure 6b shows that the MB adsorption capacity increases with the pH value, which is perfectly consistent with the surface charge results of MGHC-SA. Notice, the large difference in the adsorption performance at acidic and alkaline systems gives MGHC-SA ability which is able to precise regulate adsorption/ desorption process of MB via changing pH.

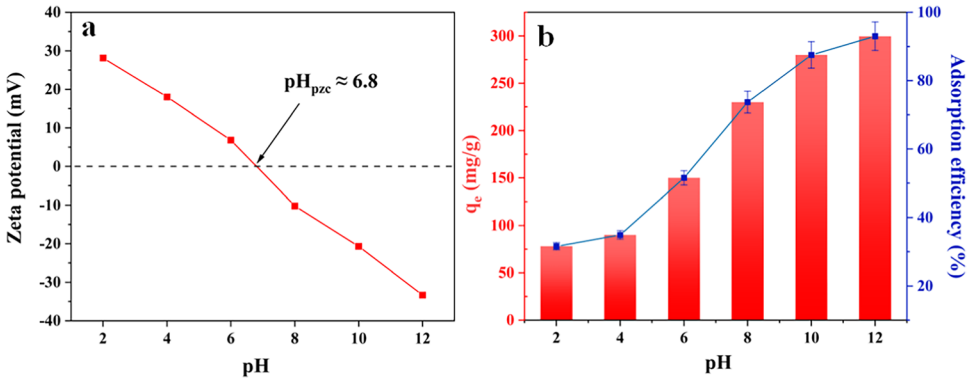

Fig. 6 **a** Zeta potential of MGHC-SA. (**b**) Effect of pH on MB adsorption (C0 = 200 mg/L, V = 50 mL, m = 30 mg, and T = 298 K)

Adsorption kinetics

The adsorption kinetics was examined to identify the effect of MGHC-SA for MB removal. At first, the curves of adsorption capacity variation of MGHC-SA with different initial MB concentration (100 to 600 mg/L) and time show that MGHC-SA can reach the adsorption equilibrium in a short time, regardless of initial concentration of MB (Fig. 7a), which suggests the rapid adsorption rate and high capacity of MGHC-SA. Then, pseudo-first-order and pseudo-second-order kinetic models were applied to simulate the adsorption kinetics data to probe the possible adsorption mechanism. As shown in Fig. 7b and c and Table S1, the fitted curves of the pseudo-secondary model with R^2 values of 0.993–0.920 are better than that of the pseudo-first-order model. This indicates that the adsorption rate of MB on MGHC-SA is mainly controlled by chemisorption, and the process of adsorption is mainly by electron transfer and electron sharing between the functional groups on the adsorbent surface and the adsorbate.

Adsorption isotherm

To further elucidate the adsorption performance of MGHC-SA and to investigate the adsorption mechanism,

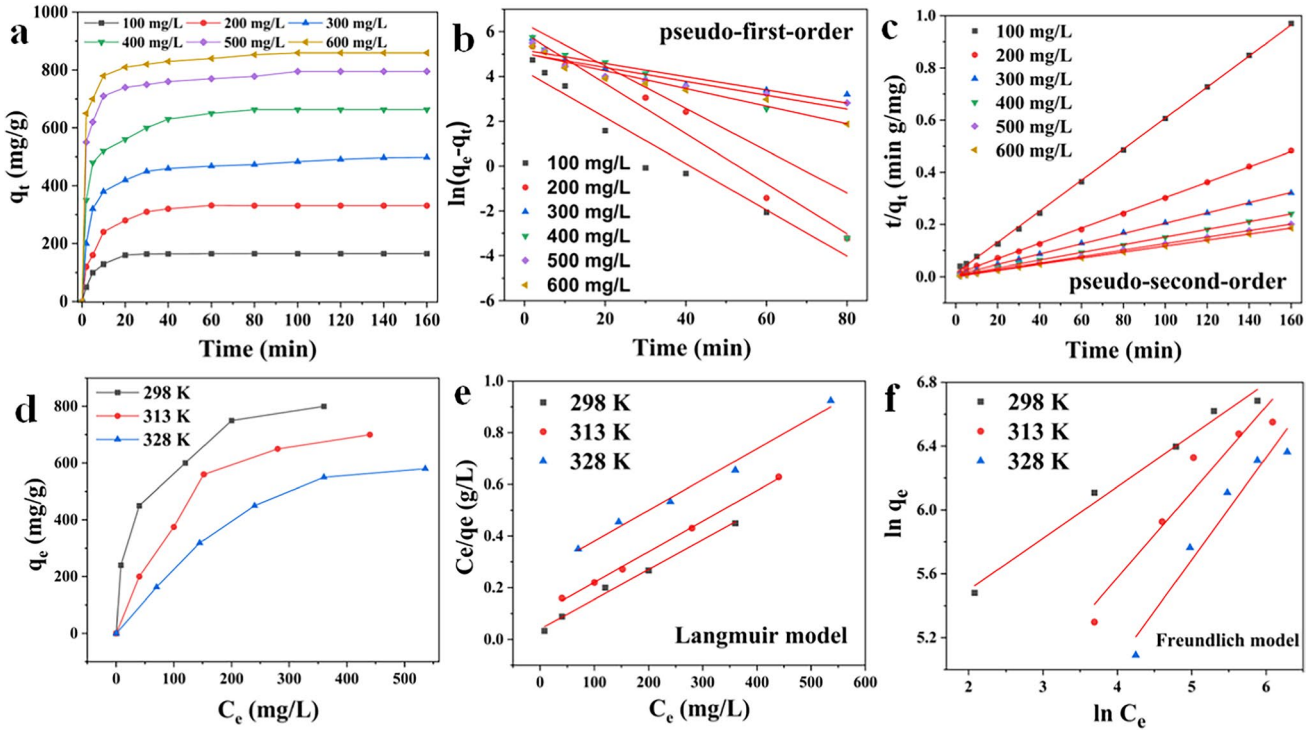

Fig. 7 **a**–**c** Adsorption kinetic model (C0 = 100–600 mg/L, V = 50 mL, m = 30 mg, t = 3 h, and T = 298 K). (d–f) Adsorption isotherm model (C0 = 600 mg/L, V = 50 mL, m = 30 mg, and T = 298–328 K)

the adsorption of MGHC-SA on MB at different temperatures ($T = 298$, 313, and 328 K) were evaluated by adsorption isotherms, and the adsorption data were fitted by Langmuir and Freundlich models. The adsorption isotherms characterize the interaction between the adsorbent and the solution when the adsorption reaches equilibrium at a constant temperature.

As shown in Fig. 7d, as the initial concentration of MB increases, there is a higher driving force at higher concentrations that promotes the diffusion of MB molecules, which in turn leads to an increase in the adsorption capacity. When the initial concentration of MB reaches a certain level, the adsorption capacity no longer increases due to the saturation of the adsorbent adsorption. It was also found that the temperature has an effect on the adsorption capacity, probably because of the enhanced thermal motion and the increased tendency of the adsorbent activity on the surface of the material desorption occurs, leading to a decrease in the adsorption capacity of the adsorbent for MB. This implies that the adsorption of MB by MGHC-SA may be an exothermic reaction, which can be carried out at room temperature.

The adsorption trend of MGHC-SA on MB is closer to the Langmuir model in Fig. 7e and f. As can be seen from Table S2, the correlation coefficients of the Langmuir model ($R2\ L > 0.987$) are better than those of the Freundlich model ($R2\ F < 0.980$), which indicates that the adsorption of MGHC-SA on MB is closer to uniform monolayer adsorption (Wang et al. 2019). In the Freundlich model, the $1/n$ values at all three temperatures were less than 1, indicating that the adsorption of MGHC-SA on MB is a spontaneous process (Li et al. 2019a). The q_{max} of MGHC-SA on MB was known to be 869.6–840.0 mg/g (298–328 K) based on Langmuir isotherm parameters, which is significantly higher than most previously reported adsorbents (Table 2). Heavy metal ions such as Cu^{2+}, Pb^{2+}, and Cd^{2+} were also selected to investigated the performance of MGHC-SA, the adsorption amounts for Cu^{2+}, Pb^{2+}, and Cd^{2+} were shown to be 34.0 mg/g, 153.3 mg/g, and 54.9 mg/g, respectively (Table S3), indicating MGHC-SA are widely applicable.

Reusability and adsorption mechanism of MGHC-SA

Adsorbent regeneration is an important part of adsorbent utilization contributing to the cost and operation convenience. According to the results of the zeta potential and adsorption capacities at different pH, MB adsorbed on the surface of MGHC-SA can be rapid desorbed in acidic condition, and MGHC-SA is regenerated. Therefore, diluted HCl (0.1 mol/L) was chosen to elute MB from the MGHC-SA. After desorption, the regenerated MGHC-SA was separated by magnet easily (Fig. S7, inset). Reusability of MGHC-SA was evaluated at pH = 11.0 and 298 K. As shown in Fig. 8, the MB adsorption capacities and removal efficiencies are maintained, even the MGHC-SA was regenerated 10 times, indicating that the active sulfonic acid groups have good bonding strength on the surface of MGHC-SA.

Adsorption mechanism of MGHC-SA

In order to investigate the adsorption mechanism of MGHC-SA on MB, FT-IR and XPS were used to characterize and analyze the interaction between surface functional groups and MB during the adsorption process of

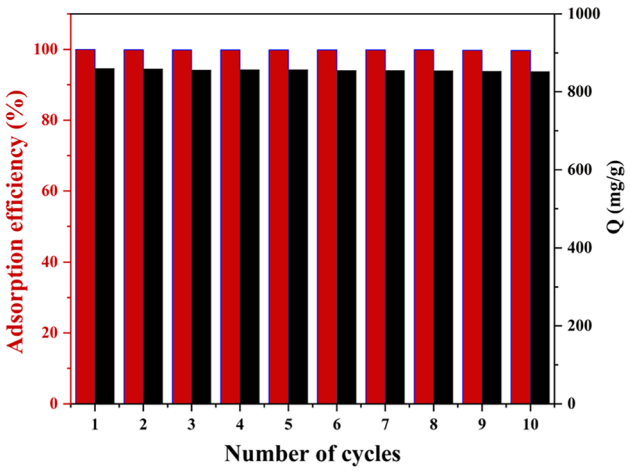

Fig. 8 The regenerative adsorption performance of MGHC-SA (C0 = 600 mg/L, V = 50 mL, m = 30 mg, pH = 11.0, t = 4 h, and T = 298 K)

Table 2 Comparison of the adsorption capacity of various biochar adsorbents for MB

Adsorbent	Q (mg/g)	T (K)	t (min)	pH	References
Ball milled biochar	310.0	303	360	-	(Zhang et al. 2021)
Bean dreg-derived carbon	4348	298	3	10	(Wang et al. 2019)
Coconut shell-derived hydrochar	200.0	303	480	9	(Islam et al. 2017)
Aloe vera–acid activated carbon	192.3	298	40	11	(Zeydouni et al. 2018)
Carbonized watermelon rind	200.0	303	300	5.6	(Jawad et al. 2019)
Polyvinyl chloride and bamboo hydrochar	258.9	308	360	11	(Li et al. 2021)
MGHC-SA	869.6	298	40	11	This work

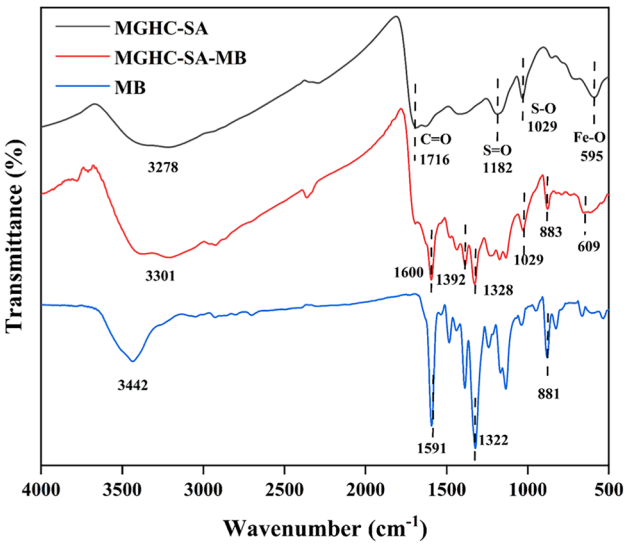

Fig. 9 FT-IR spectra of MGHC-SA, MGHC-SA-MB, and MB

MGHC-SA. FT-IR spectra are shown in Fig. 9. After the adsorption of MB, the characteristic peaks of MGHC-SA-MB appear at 1600 cm^{-1} (C = N stretching vibration), 1392 cm^{-1} (C-N stretching vibration), 1328 cm-1 (-CH_3 deformation vibration), and 883 cm^{-1} (C-H deformation vibration). The shift of the peaks indicates the adsorption of MB on MGHC-SA, which proves the interaction between MGHC-SA and MB (Li et al. 2019a). The peak changes of C = N bond (1591 cm^{-1} to 1600 cm^{-1}) and C-H bond (881 to 883 cm^{-1}) of MB indicates the presence of π–π interactions in the adsorption system (Li et al. 2021). The transfer of O–H of MGHC-SA from 3278 to 3301 cm^{-1} indicates the hydrogen bonding interaction between the nitrogen atom and the hydroxyl group (Li et al. 2018). There is also an electrostatic interaction between MGHC-SA and MB, as the C-N bond of MB on $-N(CH_3)^{2+}$ is transferred from 1322 to 1328 cm^{-1}.

The elemental composition of MGHC-SA and MGHC-SA-MB was further compared by analyzing the XPS spectra and S 2p spectra of MGHC-SA after MB adsorption (Zhang et al. 2013). As shown in Fig. 10a, the characteristic peak of N 1 s appears on MGHC-SA-MB after the adsorption of MB, indicating that MGHC-SA captures a large number of MB molecules. Figure 10b shows that the peak intensity of S 2p decreases and MGHC-SA-MB shows new characteristic peaks at 163.5 eV (S 2p3/2) and 164.7 eV (C-S/C = S) The characteristic peaks of MGHC-SA-MB at 163.5 eV (S 2p3/2) and 164.7 eV (C-S/C = S) (Xia et al. 2019) indicate that the sulfonic acid group has a strong affinity for MB adsorption. The above analysis also mirrored the FT-IR results that MGHC-SA can effectively adsorb MB.

Conclusions

In summary, in situ construction of Fe_3O_4 nanoparticles during the process of hydrothermal carbonization of sugar molecules in water is an efficient strategy to induce HC coating on the Fe_3O_4 nanoparticles. This not only makes the MGHC having smaller particle size than raw HC and exposing plenty of OCFGs but also offers magnetic core in MGHC for easy recovery. A mass of OCFGs on the surface of MGHC provides effective grafting sites to bond sulfonic acid groups, which makes MGHC-SA exhibiting high MB adsorption rate and capacity. The highest adsorption capacity of MGHC-SA for MB is 869.6 mg/g, which is achieved at pH = 11.0 and 298 K. Moreover, the high bond strength between sulfonic acid groups and adsorbent results in the good reusability of MGHC-SA, no degradation in adsorption performance was observed after 10 times regeneration. This work provides a promising strategy to prepare of high-density sulfonic acid-based magnetic HC with good MB removal performance from sugar-rich wastewater.

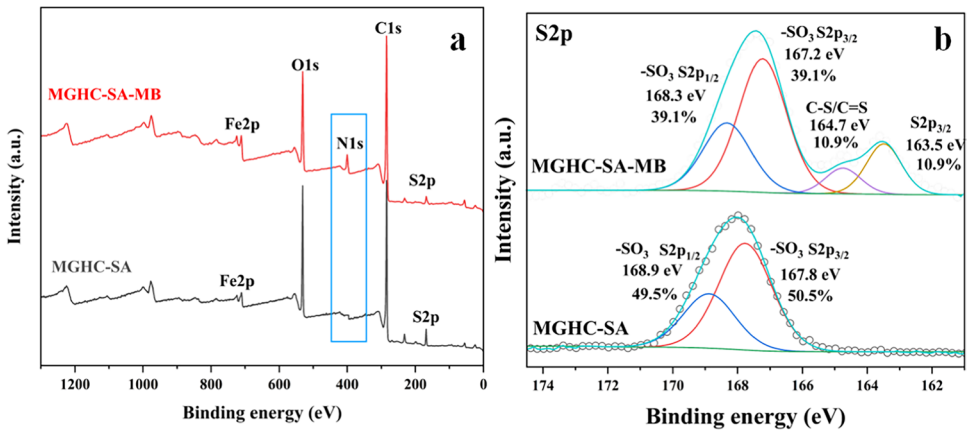

Fig. 10 **a** XPS and (**b**) S 2p spectra of MGHC-SA and MGHC-SA-MB

Supplementary Information The online version contains supplementary material available at https://doi.org/10.1007/s11356-022-24900-x.

Acknowledgements We thank the all reviewers and editors for reviewing the manuscript and providing valuable comments.

Author contribution All authors contributed to the study conception and design. Xuelei Jiang: conceptualization, methodology, validation, investigation, and writing—original draft. Yuyao Jia: investigation, visualization, methodology, formal analysis, and data curation. Dezhang Ren: data curation, writing—review and editing, and project administration. Nahui Zhang: investigation and data curation. Tao Peng: investigation and data curation. Zhibao Huo: conceptualization, supervision, project administration, writing—original manuscript, review and editing, and funding acquisition. All authors commented on previous versions of the manuscript. All authors read and approved the final manuscript.

Funding The authors gratefully acknowledge the financial support from Shanghai Pujiang Program (20PJ1404800).

Data availability Data are available upon request.

Declarations

Ethical approval This is not applicable.

Consent to participate This is not applicable.

Consent to publication This is not applicable.

Competing interests The authors declare that they have no known competing financial interests or personal relationships that could have appeared to influence the work reported in this paper.

References

Anuma S, Mishra P, Bhat BR (2021) Polypyrrole functionalized Cobalt oxide Graphene (COPYGO) nanocomposite for the efficient removal of dyes and heavy metal pollutants from aqueous effluents. J Hazard Mater 416:125929

Bhadra BN, Jhung SH (2020) Remarkable metal–organic framework composites for adsorptive removal of nitrogenous compounds from fuel. Chem, Eng. J, p 398

Caldera Villalobos M, Peláez Cid AA, Herrera González AM (2016) Removal of textile dyes and metallic ions using polyelectrolytes and macroelectrolytes containing sulfonic acid groups. J Environ Manag 177:65–73

Cheng L, Ji Y, Liu X (2021) Insights into interfacial interaction mechanism of dyes sorption on a novel hydrochar: Experimental and DFT study. Chem. Eng, Sci, p 233

Dash S, Chaudhuri H, Gupta R, Nair UG (2018) Adsorption study of modified coal fly ash with sulfonic acid as a potential adsorbent for the removal of toxic reactive dyes from aqueous solution: kinetics and thermodynamics. J Environ Chem Eng 6:5897–5905

Deng J, Li X, Wei X, Liu Y, Liang J, Tang N, Song B, Chen X, Cheng X (2019) Sulfamic acid modified hydrochar derived from sawdust for removal of benzotriazole and Cu(II) from aqueous solution: adsorption behavior and mechanism. Bioresour Technol 290:121765

Dong X, Lin Y, Ren G, Ma Y, Zhao L (2021) Catalytic degradation of methylene blue by Fenton-like oxidation of Ce-doped MOF. Colloids Surface A 608:125578

Fang R, Lu C, Zhong Y, Xiao Z, Liang C, Huang H, Gan Y, Zhang J, Pan G, Xia X, Xia Y, Zhang W (2020) Puffed rice carbon with coupled sulfur and metal iron for high-efficiency mercury removal in aqueous solution. Environ Sci Technol 54:2539–2547

Gao R, Fu Q, Hu H, Wang Q, Liu Y, Zhu J (2019) Highly-effective removal of Pb by co-pyrolysis biochar derived from rape straw and orthophosphate. J Hazard Mater 371:191–197

Goswami M, Phukan P (2017) Enhanced adsorption of cationic dyes using sulfonic acid modified activated carbon. J Environ Chem Eng 5:3508–3517

Gusain R, Kumar N, Ray SS (2020) Recent advances in carbon nanomaterial-based adsorbents for water purification. Coord. Chem, Rev, p 405

Han B, Zhang E, Cheng G, Zhang L, Wang D, Wang X (2018) Hydrothermal carbon superstructures enriched with carboxyl groups for highly efficient uranium removal. Chem Eng J 338:734–744

He P, Zhao X, Luo F, Zhang Y, Wei J, Xu T, Wu J, Chen N (2020): Magnetically recyclable Fe_3O_4 doped flower-like MoS_2: efficient removal of elemental mercury. Fuel 282:118728

Higgins LJR, Brown AP, Harrington JP, Ross AB, Kaulich B, Mishra B (2020) Evidence for a core-shell structure of hydrothermal carbon. Carbon 161:423–431

Islam MA, Ahmed MJ, Khanday WA, Asif M, Hameed BH (2017) Mesoporous activated coconut shell-derived hydrochar prepared via hydrothermal carbonization-NaOH activation for methylene blue adsorption. J Environ Manage 203:237–244

Ismail GA, Sakai H (2022) Review on effect of different type of dyes on advanced oxidation processes (AOPs) for textile color removal. Chemosphere 291:132906

Javanbakht V, Mohammadian M (2021) Photo-assisted advanced oxidation processes for efficient removal of anionic and cationic dyes using bentonite/TiO_2 nano-photocatalyst immobilized with silver nanoparticles. J. Mol, Struct, p 1239

Jawad AH, Razuan R, Appaturi JN, Wilson LD (2019) Adsorption and mechanism study for methylene blue dye removal with carbonized watermelon (Citrullus lanatus) rind prepared via one-step liquid phase H_2SO_4 activation. Surf Interfaces 16:76–84

Karray R, Karray F, Loukil S, Mhiri N, Sayadi S (2017) Anaerobic co-digestion of Tunisian green macroalgae Ulva rigida with sugar industry wastewater for biogas and methane production enhancement. Waste Manag 61:171–178

Kumar P, Kumar V, Singh J, Kumar P (2021) Electrokinetic assisted anaerobic digestion of spent mushroom substrate supplemented with sugar mill wastewater for enhanced biogas production. Renew Energy 179:418–426

Li M-x, Li A-j, Sun Q, Jiang X-m, Chen S-h (2016) Enhancement of biodiesel production by cultivating Dipodascaceae moderated-filamentous granular sludge with sugar-containing wastewater. Int Biodeterior Biodegrad 110:38–45

Li C, He Y, Zhou L, Xu T, Hu J, Peng C, Liu H (2018) Fast adsorption of methylene blue, basic fuchsin, and malachite green by a novel sulfonic-grafted triptycene-based porous organic polymer. RSC Adv 8:41986–41993

Li B, Lv JQ, Guo JZ, Fu SY, Guo M, Yang P (2019a) The polyaminocarboxylated modified hydrochar for efficient capturing methylene blue and Cu(II) from water. Bioresour Technol 275:360–367

Li L, Huang S, Wen T, Ma R, Yin L, Li J, Chen Z, Hayat T, Hu B, Wang X (2019b) Fabrication of carboxyl and amino functionalized carbonaceous microspheres and their enhanced adsorption behaviors of U(VI). J Colloid Interface Sci 543:225–236

Li Y, Tsend N, Li T, Liu H, Yang R, Gai X, Wang H, Shan S (2019c) Microwave assisted hydrothermal preparation of rice straw hydrochars for adsorption of organics and heavy metals. Bioresour Technol 273:136–143

Li H, Xu S, Wang S, Yang J, Yan P, Chen Y, Guo J, Fang F (2020) New insight into the effect of short-term exposure to polystyrene nanoparticles on activated sludge performance. J Water Process Eng 38:101559

Li HZ, Zhang YN, Guo JZ, Lv JQ, Huan WW, Li B (2021) Preparation of hydrochar with high adsorption performance for methylene blue by co-hydrothermal carbonization of polyvinyl chloride and bamboo. Bioresour Technol 337:125442

Liang H, Zhang H, Wang Q, Xu C, Geng Z, She D, Du X (2021) A novel glucose-based highly selective phosphate adsorbent. Sci Total Environ 792:148452

Liu X, Wang D, Li A (2021) Biodiesel production of Rhodosporidium toruloides using different carbon sources of sugar-containing wastewater: experimental analysis and model verification. J Cleaner Prod 323:129112

Lu Y, Hu Y, Tang L, Xie Q, Liu Q, Zhong L, Fu L, Fan C (2021) Effects and mechanisms of modified biochars on microbial iron reduction of Geobacter sulfurreducens. Chemosphere 283:130983

Luo H, Zhang Y, Xie Y, Li Y, Qi M, Ma R, Yang S, Wang Y (2019a) Iron-rich microorganism-enabled synthesis of magnetic biocarbon for efficient adsorption of diclofenac from aqueous solution. Bioresour Technol 282:310–317

Luo X, Cai Y, Liu L, Zeng J (2019b) Cr(VI) adsorption performance and mechanism of an effective activated carbon prepared from bagasse with a one-step pyrolysis and $ZnCl_2$ activation method. Cellulose 26:4921–4934

Marzbali MH, Paz-Ferreiro J, Kundu S, Ramezani M, Halder P, Patel S, White T, Madapusi S, Shah K (2021) Investigations into distribution and characterisation of products formed during hydrothermal carbonisation of paunch waste. J. Environ. Chem, Eng, p 9

Masunga N, Mmelesi OK, Kefeni KK, Mamba BB (2019) Recent advances in copper ferrite nanoparticles and nanocomposites synthesis, magnetic properties and application in water treatment: review. J. Environ. Chem, Eng, p 7

Mehmood S, Ahmed W, Rizwan M, Imtiaz M, Mohamed Ali Elnahal AS, Ditta A, Irshad S, Ikram M, Li W (2021) Comparative efficacy of raw and HNO3-modified biochar derived from rice straw on vanadium transformation and its uptake by rice (Oryza sativa L.): insights from photosynthesis, antioxidative response, and gene-expression profile. Environ. Pollut. 289:117916

Methneni N, Morales-Gonzalez JA, Jaziri A, Mansour HB, Fernandez-Serrano M (2021) Persistent organic and inorganic pollutants in the effluents from the textile dyeing industries: ecotoxicology appraisal via a battery of biotests. Environ Res 196:110956

Naeimi H, Mohamadabadi S (2014) Sulfonic acid-functionalized silica-coated magnetic nanoparticles as an efficient reusable catalyst for the synthesis of 1-substituted 1H-tetrazoles under solvent-free conditions. Dalton Trans 43:12967–12973

Oliveira AS, Cordero-Lanzac T, Baeza JA, Calvo L, Heras F, Rodriguez JJ, Gilarranz MA (2021) Continuous aqueous phase reforming of a synthetic brewery wastewater with Pt/C and PtRe/C catalysts for biohydrogen production. Chemosphere 281:130885

Phetphaisit CW, Yuanyang S, Chaiyasith WC (2016) Polyacrylamido-2-methyl-1-propane sulfonic acid-grafted-natural rubber as bioadsorbent for heavy metal removal from aqueous standard solution and industrial wastewater. J Hazard Mater 301:163–171

Pirsaheb M, Mohamadisorkali H, Hossaini H, Hossini H, Makhdoumi P (2020) The hybrid system successfully to consisting of activated sludge and biofilter process from hospital wastewater: ecotoxicological study. J Environ Manag 276:111098

Qu J, Wang S, Wang Y, Tian X, Jiang Z, Tao Y, Wang L, Deng F, Zhang Y (2021) Removal of Cd(II) and anthracene from water by beta-cyclodextrin functionalized magnetic hydrochar: performance, mechanism and recovery. Bioresour Technol 337:125428

Samuchiwal S, Gola D, Malik A (2021) Decolourization of textile effluent using native microbial consortium enriched from textile industry effluent. J Hazard Mater 402:123835

St K, Pavithran RAV (2021) Design of 3D-supramolecular metal organic framework of zinc as photocatalyst for the degradation of methylene blue through advanced oxidation process. J. Mol, Struct, p 1245

Varjani S, Rakholiya P, Shindhal T, Shah AV, Ngo HH (2021): Trends in dye industry effluent treatment and recovery of value added products. J Water Process Eng 39:101734

Viotti PV, Moreira WM, Santos OAAd, Bergamasco R, Vieira AMS, Vieira MF (2019) Diclofenac removal from water by adsorption on Moringa oleifera pods and activated carbon: mechanism, kinetic and equilibrium study. J Cleaner Prod 219:809–817

Wang J, Wang S (2019) Preparation, modification and environmental application of biochar: a review. J Cleaner Prod 227:1002–1022

Wang X, Ma C, Xiao J, Xia Q, Wu J, Li Z (2018) Benzene/toluene/water vapor adsorption and selectivity of novel C-PDA adsorbents with high uptakes of benzene and toluene. Chem Eng J 335:970–978

Wang B, Zhai Y, Wang T, Li S, Peng C, Wang Z, Li C, Xu B (2019) Fabrication of bean dreg-derived carbon with high adsorption for methylene blue: effect of hydrothermal pretreatment and pyrolysis process. Bioresour Technol 274:525–532

Wolski L, Sobanska K, Walkowiak A, Akhmetova K, Grybos J, Frankowski M, Ziolek M, Pietrzyk P (2021) Enhanced adsorption and degradation of methylene blue over mixed niobium-cerium oxide - unraveling the synergy between Nb and Ce in advanced oxidation processes. J Hazard Mater 415:125665

Wu J, Yu H, Liu W, Dong C, Wu M, Zhang C (2022) Enhanced degradation of organic pollutant by bimetallic catalysts decorated micromotor in advanced oxidation processes. J. Environ. Chem, Eng, p 10

Xia S, Huang Y, Tang J, Wang L (2019) Preparation of various thiol-functionalized carbon-based materials for enhanced removal of mercury from aqueous solution. Environ Sci Pollut Res Int 26:8709–8720

Yang Y, Cannon FS (2021) Preparation of activated carbon from pine sawdust with hydrothermal-pressure preconditioning. J Environ Chem Eng 9:106391

Yang W, Liu Y, Pan J (2021) Experimental and kinetic study on Hg^0 removal by microwave/hydrogen peroxide modified seaweed-based porous biochars. Environ. Technol, Innovation, p 22

Zeydouni G, Rodriguez Couto S, Nourmoradi H, Basiri H, Amoatey P, Esmaeili S, Saeidi S, Keishams F, Mohammadi MJ, Omidi Khaniabadi Y (2018) H2SO4-modified Aloe vera leaf shells for the removal of P-chlorophenol and methylene blue from aqueous environment. Toxin Rev 39:57–67

Zhang H, Li A, Sun J, Li P (2013) Adsorption of amphoteric aromatic compounds by hyper-cross-linked resins with amino groups and sulfonic groups. Chem Eng J 217:354–362

Zhang W, Lan Y, Ma M, Chai S, Zuo Q, Kim KH, Gao Y (2020) A novel chitosan-vanadium-titanium-magnetite composite as a superior adsorbent for organic dyes in wastewater. Environ Int 142:105798

Zhang Y, Zheng Y, Yang Y, Huang J, Zimmerman AR, Chen H, Hu X, Gao B (2021) Mechanisms and adsorption capacities of hydrogen peroxide modified ball milled biochar for the removal of methylene blue from aqueous solutions. Bioresour Technol 337:125432

Zhao W, Jiao Y, Gao R, Wu L, Cheng S, Zhuang Q, Xie A, Dong W (2020) Sulfonate-grafted conjugated microporous polymers for fast removal of cationic dyes from water. Chem, Eng. J, p 391

Zheng Y, Wang J, Li D, Liu C, Lu Y, Lin X, Zheng Z (2021) Insight into the KOH/KMnO4 activation mechanism of oxygen-enriched hierarchical porous biochar derived from biomass waste by in-situ pyrolysis for methylene blue enhanced adsorption. J. Anal. Appl, Pyrolysis, p 158